Fire Safety Journal 134 (2022) 103675

Contents lists available at ScienceDirect

Fire Safety Journal

journal homepage: www.elsevier.com/locate/firesaf

Flame heights and charring on a particle board – An experimental study

Dheeraj Dilip Karyaparambil [a,b,*], Sveinung Erland [a], Patrick van Hees [c], Vidar Frette [a], Bjarne Christian Hagen [a]

[a] Department of Safety, Chemistry and Biomedical laboratory sciences, Western Norway University of Applied Sciences, Bjørnsonsgate 45, 5528, Haugesund, Norway
[b] Department of Physics and Technology, University of Bergen, Postboks 7803, 5020, Bergen, Norway
[c] Division of Fire Safety Engineering, Lund University, P.O. Box 118, 221 00, Lund, Sweden

ARTICLE INFO

Keywords:
Particle board
Flame height
Charring
Flame spread
Facade

ABSTRACT

Vertically oriented particle-board samples were exposed to external venting flames to study the fire spread and charring behaviour along a timber façade. Variation in flame height and the height, volume, area, density, and depth of the char layer were studied to determine the impact of heat-release rate and experiment duration. There was a peak flame height after which the flame returned to steady height approximately equal to the value before the ignition of the particle board and flame heights with inert panels. Flames did not spread to the top of the panel with increased experiment duration. Char height and area were found to increase with heat-release rate but were not affected significantly by experiment duration. Char depth and volume increased with both experiment duration and heat-release rates. Char density decreased with increased experiment duration and heat-release rate.

1. Introduction

It is well-established that an externally venting flame can result in a fire spread through the façade along the height of the building. An increased usage of timber urged by the drive to attain sustainability in the built environment, including in the façade is observed recently [1–4]. However, a global increase in façade fire incidents [5] like the Grenfell tower fire in London in 2017 [6] and Torre dei Moro in Milan in 2021 [7] raises concerns for a similar incident involving a timber façade. A timber façade introduces a serious risk of fire spread along the façade to upper floors, to other compartments in the same floor and to neighbouring buildings since timber has a high heat of combustion and undergoes pyrolysis at around 200 °C [8]. Therefore, safe application of timber as a façade element in a building requires substantial knowledge of its fire behaviour.

As stated previously, external venting flames can result in fire spread along the façade of a building. Asimakopoulou et al. [9] studied the characteristics of externally venting flames and their effect on the façade using fire-resistant samples and an *n*-hexane pool fire as the fuel source. The study suggested three phases of external venting flames, namely "internal flaming", "intermittent flame ejection" and "consistent external flaming". It was observed that the external flaming phase had the largest duration of them all, which emphasizes the importance of further understanding the façade behaviour during this phase. Sun et al. [10] investigated the height of external venting flames ejected through an opening with fire resistant boards representing façades and a gas burner with gradually increasing heat-release rate to simulate fire growth from over-to under-ventilated conditions inside the compartment. Replacing the fire-resistant samples with combustible timber samples will result in vertical fire-spread initiated by external venting flames, which was not investigated by Asimakopoulou et al. [9] or Sun et al. [10].

Fire spread on a timber façade could be simplified to a vertical fire spread problem along a charring, timber/timber-based panel like particle board. Saito et al. [11] and Brehob and Kulkarni [12] studied the upward flame spread along particle board and observed that there was no sustained fire propagation across the height of the sample, even when the burner remained on throughout the experiment. Optimal conditions for fire spread occurred when the flame height was larger than the pyrolysis height. Brehob and Kulkarni [12] also recorded the flame height but did not use any backing material for their sample or study the charring behaviour of the samples. Kasymov et al. [13] studied vertical temperature profiles across the height of timber-based samples and estimated the upward fire spread rate which varied from 0.8 ± 0.15 mm/s for chipboard to 1.38 ± 0.33 mm/s for plywood. Koutaïba et al. [14], using timber panels, studied the temperature profile along the

* Corresponding author. Western Norway University of Applied Sciences, Bjørnsonsgate 45, 5528, Haugesund, Norway.
E-mail address: dhdk@hvl.no (D.D. Karyaparambil).

https://doi.org/10.1016/j.firesaf.2022.103675
Received 8 April 2022; Received in revised form 26 August 2022; Accepted 22 September 2022
Available online 26 September 2022

height at the centreline of the sample as well and the charring depth along the height of the sample. However, Koutaïba et al. did not measure flame height evolution over time or the effect of varying heat-release rate and exposure time on char features.

Definition and measurement of flame height in laboratory experiments vary over literature. Zukoski [15] defined mean flame height as the part of the flame with an intermittency of 50%, i.e., the height at which the flame appears half of the time. Lee et al. [16] and Sun et al. [10] interpreted flame heights as the height of 50% intermittency as well and measured it from the neutral plane at the fire compartment opening. Sjöström et al. [17] determined flame height on an inert façade excluding *flamelets* (detached flames) by only considering the flames with largest area in each frame. Consalvi et al. [18] investigated methods to measure flame heights and concluded that the continuous flame (region where flames are present all the time) does not give an appropriate representation of flame height for combustible materials and that flame height based on the heat flux incident on the sample surface is more reliable. Later, Hu et al. [19] and Asimakopoulou et al. [20] presents flame height as time averaged flame intermittency distribution.

Char features have less ambiguous definitions compared to flame height. As highlighted by Buchanan and Abu [21], charring in timber which happens around 300 °C due to rapid pyrolysis is different from slower pyrolysis that could occur around 200 °C. Friquin [22] reviews that most research considered 300 °C as the char front boundary. Bartlett et al. [8] dissects the different processes that happen before and during charring and shows that these processes are not perfectly bound within the temperature range. According to Friquin [22], this temperature range is dependent on the species of timber, moisture content and heating rate. Measuring in-depth sample temperature during the experiment usually require installation of thermocouples inside the sample like in experiments by Emberley et al. [23]. If this is not possible due to practical limitation or scope of research, an alternate is to measure the char depth after the experiment like Xu et al. [24]. Char height and area are straightforward measurements once their definitions are established. However, while char height could be defined as the highest location on the vertical sample surface that has undergone pyrolysis at around 300 °C and char area as the area of this pyrolyzed region, a visual distinction of the region that had undergone pyrolysis at 200 °C and 300 °C could be difficult.

Many other previous research, including some full-scale tests, had focused on significant physical behaviours related to façade fires [25–28]. However, few of the above studies explored the coupling between the fire-spread dynamics of external venting flames and the charring behaviour. A detailed quantification of variation in flame heights and char behaviour on the sample with heat-release rate in the fire compartment and experimental duration was not documented in any of them. This study focuses on external vertical fire spread along a timber façade from post-flashover flames emerging through a window below. Particular attention is given to variations in charring behaviour with flame height and experiment duration, and how it affected upward flame spread on particle boards. The findings may be used to design safer timber façades reducing the risk of fire spread away from the fire compartment.

Nomenclature

a_c	Char area (mm^2)	H	Height of the ventilation opening (m)
A_T	Area of walls and ceiling of compartment excluding ventilation opening and floor (m^2)	$\dot{Q}$	Heat-release rate (kW)
A_W	Area of ventilation opening (m^2)	t_{exp}	Experiment duration (min)
d_{ch}	Char depth (mm)	V_{ch}	Char volume (mm^3)
d_{avg}	Average char depth	$x_{f,5}$	Flame height from 5s moving average (mm)

(*continued on next column*)

(*continued*)

Nomenclature

h_0	Height where char depth = 0	$x_{f,peak}$	Peak flame height from 5s moving average (mm)
h_{ch}	Visible char height (mm)	ρ_{ch}	Char density (kg/m^3)
h_{ch^*}	Measurable char height (depth >1 mm) (mm)		

2. Material and methods

The objective of this study is to investigate the fire spread and charring on a vertical particle board panel resulting from an imposed flame under varying heat-release rate in the fire compartment and experimental duration. The experimental setup was designed to mimic a scenario with a room under post-flashover conditions with external flames venting through a window and incident onto a timber façade, causing fire spread to the floors above. The sample represented the spandrel zone between the windows of two consecutive floors.

2.1. Setup

The particle boards (1200 × 600 × 22 mm) were attached to an inert (calcium silicate) back panel mounted on a wooden frame and placed vertically on top of the fire compartment. As shown in Fig. 1, the fire compartment was made of light-weight concrete and had the dimensions 400 (length) × 200 (width) × 400 (height) mm. The opening was 200 (width) × 400 (height) mm with an opening factor (as defined by Thomas [29]) of 9.5 m$^{-1/2}$, which allowed for high temperature and stable combustion under ventilation-controlled conditions, as observed during the experiments. The opening factor was calculated according to equation (1) [29],

$$\text{Opening factor} = \frac{A_T}{A_W H^{1/2}} \tag{1}$$

where A_T is the total area of the compartment boundaries excluding the floor and ventilation opening, A_w is the area of ventilation opening and H is the height of the opening. The fire compartment was designed without a soffit or head space above the opening. A gas burner of size 100 × 100 × 100 mm was placed inside the fire compartment. The bottom side of the panels were flush to the roof of the fire compartment and further gaps were filled with silicate push strips [30].

16 type K thermocouples (1 mm including shielding) were placed along the centre of the surface of the panel with ~80 mm vertical spacing (Fig. 1) with no radiation correction. The thermocouples were placed about 1–2 cm away from the surface of the panel and were attached to the frame that supported the sample. They were not attached to the panel to prevent any effects on the surface behaviour. Thermocouples were used to study the temperature evolution along the height of the sample.

3. Materials

Particle boards were selected for the experiments due to a low degree of deformation during the fire and negligible response to changes in air-moisture content: their mass varied maximum 0.3% in the lab environment over a 9-day period. The particle boards used had sanded surfaces without any other surface finishing as reported by the manufacturer. Babrauskas and Parker [31] tested Douglas-fir particle boards with cone calorimeter and reported a minimum heat flux for ignition of 25 kW/m^2. Lateral Ignition and Flame spread Tests (LIFT), Reduced scale Ignition and Flame Spread Test (RIFT) and ISO 5657-1987 Ignition Apparatus tests were carried out for a pine-based particle board (similar to the sample used for this study) by Merryweather and Spearpoint [32, 33], who reported minimum heat flux for ignition that varied between

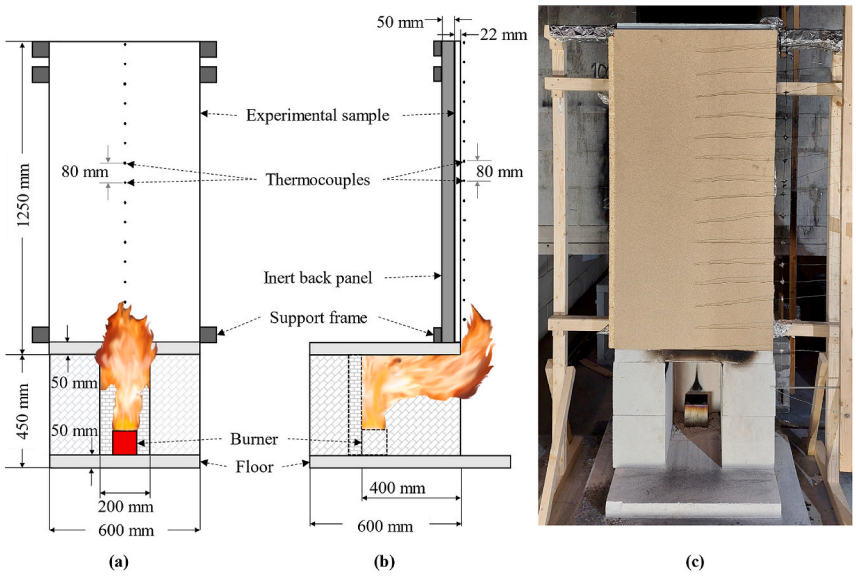

Fig. 1. Experimental setup. (a) Front view with thermocouples indicated as dots along the panel. (b) Side view of the experimental setup with the 400 mm long fire chamber and the inert back panel. The thermocouples did not touch the sample. (c) Photo of the experimental setup from the front.

13.75 and 24.9 kW/m^2. Inert panels were used as samples in some experiments to isolate the contribution of flames from the particle board. Further details of the sample materials are provided in Table 1. Material data that is not reported by suppliers have been taken from literature.

Propane was used as fuel, with flow rates 0.5, 0.6, 0.7 and 0.8 g/s (± 0.006 g/s), regulated using a mass-flow controller. The heat-release rates corresponding to the gas flow rates, assuming 100% combustion efficiency and a constant heat of combustion of 46.45 kJ/g [39], are ~23, 28, 33 and 37 kW respectively. These values are used here as reference values, and do not represent true heat fluxes towards the panels, since a part of the gas is burned inside the compartment and there will be heat losses from conduction through the walls, evaporation of moisture in the compartment, convection, and radiation to surroundings. Direct measurement of the heat flux to the panels have not been carried out during the experiments to be reported here. The gas flow remained unchanged throughout each experiment. The lowest gas flow rate used was 0.5 g/s (the lowest flow rate that ignited the panel) and the highest flow rate was 0.8 g/s (flow rates above that burned down the panel quite fast and flames extended to the rear side of the panel). Experiments were conducted for 15, 20 and 25 min. The minimum duration was set to 15 min as most of the experiments at 0.5 and 0.6 g/s had their maximum flame heights (see Fig. 10) after or around 10 min, while experiments beyond 25 min had the panels burned through significantly and left the panel too deformed to make reliable char-depth measurements. Five-minute intervals in experimental duration were selected based on preliminary experiments to obtain measurable differences in data.

Table 1
Material data.

	Particle board panel [34,35]	Inert panel [36]	Aerated concrete [37,38]
Components	~84% timber (Norway spruce and pine), ~9% glue and ~7% water	calcium silicate	sand, lime, and water
Thickness (m)	0.022	0.05	0.2 (walls) & 0.05 (roof)
Density (kg/m^3)	~700	225	290 ± 10
Thermal conductivity (W/(m·K))	0.13	0.074	0.076
Specific heat capacity (J/(kg·K))	1420–1450	840	1050

3.1. Experimental procedure

A total of 80 experiments were carried out, 60 with particle boards and 20 with a calcium silicate (inert) panel. Table 2 shows all the gas flowrates and durations used for the experiments.

The panels were weighed before and after the experiment to estimate the total mass lost. They were then mounted on to the frame. Data logging for thermocouples started at 0 s, video recording at 30 s, and the gas flow at 60 s. Once the gas flow was initiated, there was about 13 s delay before it was ignited, and the flames appeared outside the fire compartment. The ignition time of the panel was noted visually, and the experiment was terminated after predetermined times 15, 20 or 25 min. A few experiments with 23 kW for 15 min had flaming on the panel even

Table 2
Experimental overview.

Material	Gas flow (g/s)	Heat-release rate, $\dot{Q}$ (kW)	Experimental duration (min)	Total no. of experiments
Particle board	0.8	37	25	20
	0.7	33		
	0.6	28		
	0.5	23		
	0.8	37	20	20
	0.7	33		
	0.6	28		
	0.5	23		
	0.8	37	15	20
	0.7	33		
	0.6	28		
	0.5	23		
Inert (Calcium silicate)	0.8	37	25	16
	0.7	33		
	0.6	28		
	0.5	23		
	0.8	37	15	4
	0.7	33		
	0.6	28		
	0.5	23		

after the gas was turned off. These flames were manually extinguished after the gas was turned off. Five experiments were conducted for each set of parameter values, see Table 2.

3.1.1. Procedure for measurement of flame heights

Flame heights of the externally venting flames from the compartment were measured and compared with the charring behaviour of the panel. As both the connected flame and flamelets will transfer heat to the sample, flame height in this study will include the flamelets; flame height is the highest point where combustion is observed, as measured from the bottom of the sample panel. This gives a better measure of the degree of pyrolysis of an upward spreading flame than mean height of the connected flame or the flame intermittency model. The measurement in Fig. 2 included detached flames and not just the connected ones.

Flame heights were measured from the video frames after extracting the red channel from each RGB frame, and then binarizing the extracted frame through Otsu method [40] using a binarization factor, similar to previous research [41,42]. The binarization factor (threshold value for converting a frame into a binary image) was determined based on the brightness and reflection from the background in preliminary experiments. Flame height was obtained from the highest pixel in the video frame with a value larger than 128 (0.5 binarization factor), as shown in Fig. 2, using computer software. To avoid noise due to reflection from the burning panel and flicker flames, only binarized flames with an area above 1 cm^2 were considered. Flame heights higher than the sample were recorded as 1200 mm. Shutter speed, ISO speed and aperture value of the camera were optimized for the lab environment. The optical axis of the camera was perpendicular to the surface of the sample panel, and a static pixel-to-meter conversion (each pixel was assumed to be covering the same amount of area on the panel) was used. The camera was placed ~4 m (maximum distance possible in the lab) away from the panel and perspective errors were found negligible. The height of the centre of the lens from the floor was set in such a way that the optical axis was in line with the centre of the sample panel, as shown in Fig. 3. The camera settings are shown in Table 3.

3.1.2. Procedure for measurements of char layer

Exposure to flames resulted in a charred layer on the sample extending upwards from the bottom. After the end of each experiment, the char height (h_{ch}) was measured as the highest point on the panel with visible surface ruptures. It was measured manually using a measuring tape, and the charred area (a_{ch}) was marked to facilitate measurement from images using a computer program. A month after the experiments, the char was removed manually using a chipping hammer leading to samples, as shown in Fig. 4 (b), to measure the char depth (d_{ch}) and volume (V_{ch}) from the sample panels. The sample was weighed before and after char removal to estimate the mass of the removed char.

To determine the geometry of the charred region and measure char

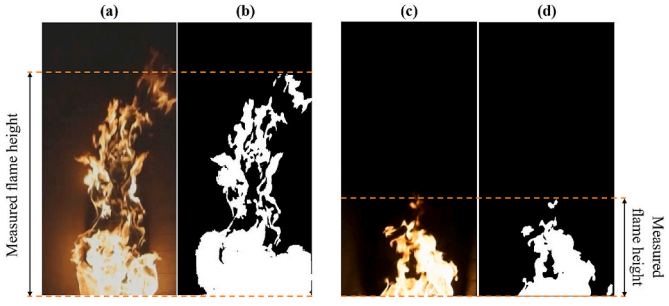

Fig. 2. Flame height measured as the highest point of a flame. Video frames for a particle board (a) and inert panel (c) at 37 kW are shown along with their binarized frames (b) and (d), respectively. In (a) and (b) the flame height is partially due to the contribution of pyrolysis gases from the sample while in (c) and (d) all the flame height is caused by the propane.

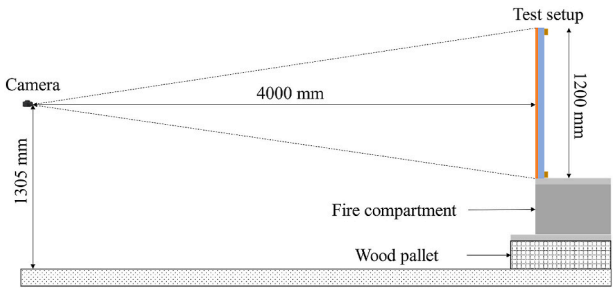

Fig. 3. Camera positioning relative to the sample panel (to scale).

Table 3
Camera settings.

Camera model	Canon EOS 7D Mark II
Image sensor	22,4 x 15,0 mm CMOS
Shutter speed	1/250
Aperture value	1.8
Metering mode	Centre-Weighted Average Metering
Exposure compensation	0
Iso speed	100
Auto ISO speed	OFF
Lens	18–35 mm
Focal length	35.0 mm
Image size (pixels)	1920x1080
Movie exposure	Manual
Frame rate (frames per second)	24

depth, a grid panel with perforations on the nodes of a 50 × 50 mm grid as shown in Fig. 5 was constructed. The sample was sandwiched between a back plate (18 mm thick) at bottom and the grid panel at top, as shown in Fig. 6. Measurements were made using the depth rod on a digital vernier calliper. The volume of the removed char was measured for every "cell" by considering it as a cube of dimensions 50 (length) × 50 (width) × *height* mm. The height was calculated as the average of the depth measured at the four enclosing nodes of the grid (edges of the cell).

4. Results

4.1. A representative experiment

Following the ignition of the panel, there was a peak flame height after which the flames receded to a relatively stable height similar to the one before ignition, as was also demonstrated by previous studies [11,12,43]. To reduce the noise, a 5 s (120 data points) moving average was applied. All the flame height analysis was based on these averaged data points. Fig. 7 shows various stages in a typical experiment through the flame height $(x_{f,5})$ (I) and characteristic images (II).

In Fig. 7 (I), regime 1, the sample is exposed to flames and its surface temperature increases. In regime 2, the panel is ignited, leading to flames that extend much higher on the panel. Eventually, a peak value is reached for the flame height (Fig. 7 (II)(c)). The heat transfer responsible for fire spread happens in the region above the already pyrolyzed region [11], and when the heat flux from the flames is not high enough to pyrolyze the region above, the flame spread stops (further explained in the Discussion). Once the char layer starts to develop, restricting heat transfer into the sample, a gradual reduction in pyrolysis-gas production due to exhaustion of exposed virgin fuel occurs, lowering the flame height (regime 3). In regime 4 (Fig. 7 (II)(d)), further exposure of the charred layer led to formation of cracks, resulting in secondary flaming and in-depth charring of the sample.

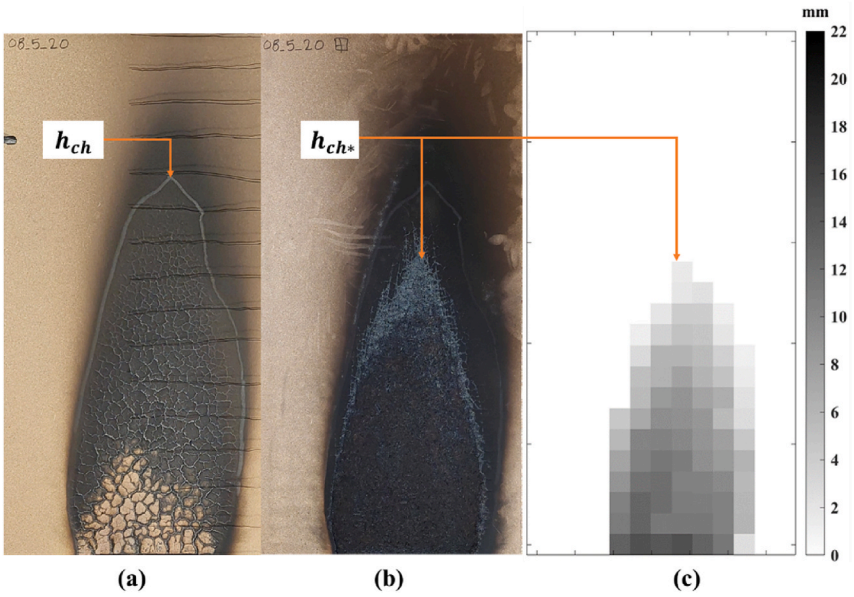

Fig. 4. Panel after the experiment (a) before and (b) after char removal, along with (c) a representation of the char depth (d_{ch}), distribution. Point marked in (a) shows the char height, h_{ch} (highest point of surface deformation) and the one in (b) shows the measurable char height (depth >1 mm) (mm), (h_{ch*}). Note the white char in (a), which represented higher d_{ch}, as shown in (c).

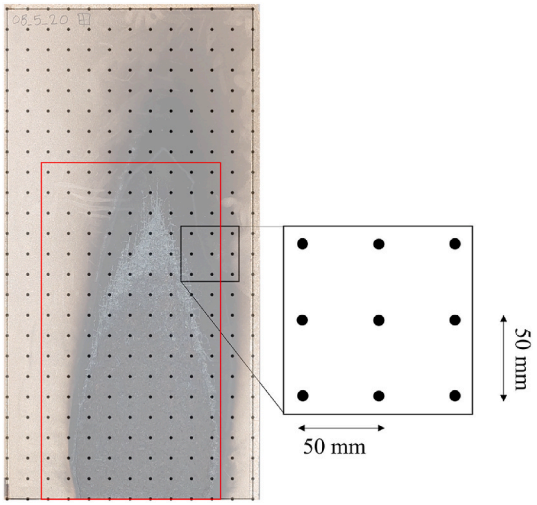

Fig. 5. Grid for char-depth measurement (top view). From preliminary analysis, only the area inside the region marked in red had measurable charring. (For interpretation of the references to colour in this figure legend, the reader is referred to the Web version of this article.)

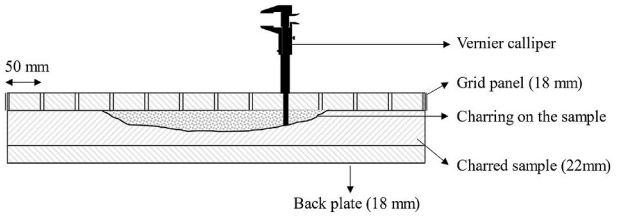

Fig. 6. Char-depth measurement setup (side view at the lower edge of the panel, as mounted during the experiment). See explanation in the main text.

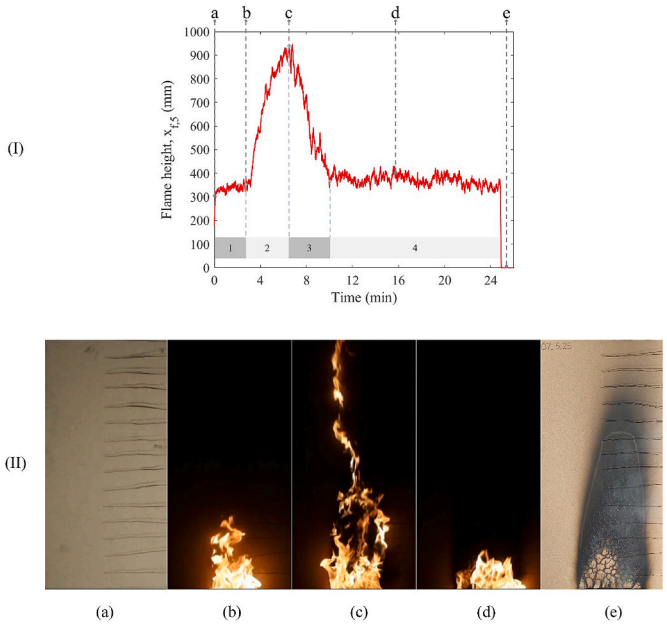

Fig. 7. Flame heights during a representative experiment for heat-release rate 33 kW and with an experimental duration of 25 min. (II): Images of the panel: (a) Before the experiment started, (b) before ignition of the panel, (c) during the peak flaming phase, (d) after the flames receded to a steady-state, and (e) after the experiment. The times of the five cases in part II are indicated by vertical lines in part I.

4.2. Flame heights

In separate experiments with inert panels, flame heights were determined in the absence of any combustible material. Through comparison with flame heights in experiments on combustible panels, the contribution to the flame from pyrolysis gases could be isolated. Fig. 8 shows the flame heights ($x_{f,5}$) on the inert panel for the different heat-release rates. For each rate, four experiments were averaged. Each curve displays an increase during the first 2 min as the plate is getting

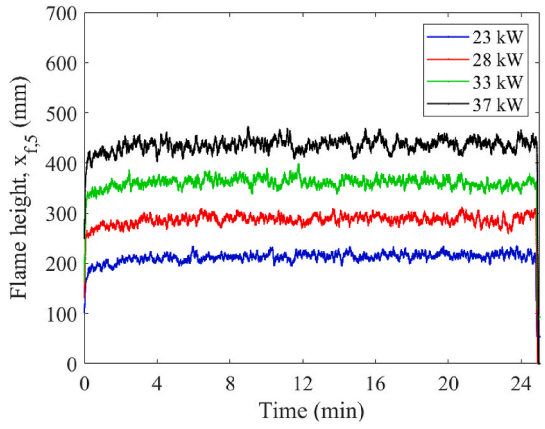

Fig. 8. Comparison of averaged flame height for different heat-release rates with an inert panel.

heated, followed by an approximately constant value during most of the experiment. There was an increase in average flame height by 76 ± 2 mm for every 4–5 kW (0.1 g/s propane flow rate) increase in heat-release rate.

Fig. 9 compares the flame heights on an inert and a particle-board panel. The significant increase in flame height observed around 3.5 min is due to ignition of the particle-board panel, followed by a peak around 6.5 min. The flame heights then recede back to values close to those of the inert panel, as shown in the figure. This trend was observed in all the experiments.

The gas-flow rates used delivered relatively stable and measurably distinct flame heights as demonstrated in Fig. 8. Fig. 9 shows the contribution from particle boards to flame height compared with an inert panel where the propane gas alone was responsible for the flame height. In Fig. 9, the flame heights for the particle board are lower than for the inert panel before ignition of the panel. This behaviour was observed for all the experiments, and it may be due to differences in material properties (see Table 1). Inert panels conduct much less heat from the surface into the panel compared with particle boards due to lower thermal conductivity. This would imply that the surface of an inert sample is hotter than a particle board before ignition, causing increased convective flows resulting in higher flames. This difference in temperature is demonstrated in the discussion section (see Fig. 26).

Fig. 10 shows the flame height evolution for all the experiments with duration of 25 min for particle-board panels. Each figure part displays the run-to-run variations at fixed heat-release rate. These variations decrease for higher heat-release rate. Fig. 11 shows typical variations

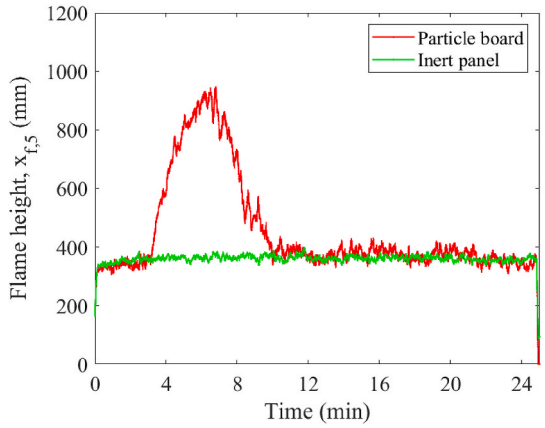

Fig. 9. Comparison of flame height on inert panel and particle board, both with a heat-release rate of 33 kW and duration 25 min. The particle-board experiment is the same as shown in Fig. 7.

between different heat-release rates. The plateau (steady-state) flame height (before and after the peak) increases with heat-release rate. For some experiments, secondary burning was observed with a smaller peak than the peak flame height (see e.g., Fig. 10 (b)). Secondary burning could result from cracks in charred surface that expose fresh fuel to the flame (further explained in the Discussion).

Brehob and Kulkarni [12] measured flame heights on vertical particle board sample as well. The peak flame height attained by the samples without additional external radiation was reported as ~600 mm and initial flame height was ~250 mm, which are comparable to the 23 kW experiments in this study (see Fig. 11).

Since the panels did not ignite with 18 kW (0.4 g/s), the minimum heat flux for ignition must correspond to heat-release rates between 18 and 23 kW and explain why ignition times with 23 kW exhibited a wide variation (324–812 s), as shown in Fig. 10 (a).

Figs. 10 and 11 indicate increase in peak flame heights with heat-release rate. This impact of heat-release rates on peak flame height ($x_{f,peak}$) and steady-state flame height is further illustrated in Fig. 12. The peak flame heights increased with heat-release rates (propane flowrate) as expected, and the increase is approximately linear. Data points for peak flame heights in Fig. 12 are the peak value from moving-average flame height plots (Fig. 10) similar to point 'c' in Fig. 7 (I). Data points for steady-state are taken as the average steady-state flame height after the peak from the moving-average plots (similar to average of regime 4 in Fig. 7 (II)). Peak flame heights had higher variation than steady-state flame height under the same heat-release rate. Steady-state flame heights occur in the region of the sample where most of the fuel had already been burnt off during the peak flaming period. Meanwhile, the peak flame height occurs in the region of the sample where the available fuel has a higher degree of variation. In Fig. 12, the standard deviation for the steady-state flame height between the experiments varies from 8.8 to 16.8 mm, increasing with heat-release rate. Notice that the standard deviation for the flame height within each experiment is about twice as high and is increasig with heat-release rates since there are larger and more frequent secondary peaks (see Fig. 10).

Fig. 13 shows the comparison of steady-state flame height data with results of Lee et al. [16]. Lee et al. used a non-combustible façade material and defined flame heights using intermittency levels. Since Lee et al. used an inert panel and, since in this study the steady-state flame heights resembled flame heights with inert panels, it is logical to compare the results. However, despite the many differences in methodology and setup, a similar trend for flame height evolution is observed between the studies.

The duration of the peak in flame height (time between ignition and recession back to steady-state flame heights), except for 23 kW at 15 min, varied between 3 min and 7 min with a mean of 5 min (data not shown).

The approximate rate of fire spread and the subsequent flame decay to steady-state flame heights were estimated from the moving-average graph. Flame spread rate was calculated from the peak flame height achieved and the duration to achieve peak flame height after ignition, while the decay rate was calculated from the duration taken to reach steady-state from the peak flame height. The flame-spread rate varied between 1.7 and 4.9 mm/s, with an average of ~3.2 ± 0.91 mm/s. The decay rate varied from 0.87 mm/s to 5.47 mm/s, with a mean value of ~2.47 ± 1 mm/s. Fire spread rate should increase with heat-release rate since the incident heat flux on the sample surface will also increase resulting in an accelerated spread. However, within the range of parameters used in this study, impact of heat-release rate (23–37 kW) on fire spread and decay rates could be considered statistically insignificant since the p-value was greater than 0.05. The heat-release rate had a clear impact on the peak flame height but not on the rate at which that flame height was achieved nor the rate at which it decayed to the steady-state value. Overall, both flame-spread rate and flame-decay rate display significant variations between experiments. Decay rates are lower than spread rates, which is not surprising since different mechanisms are in

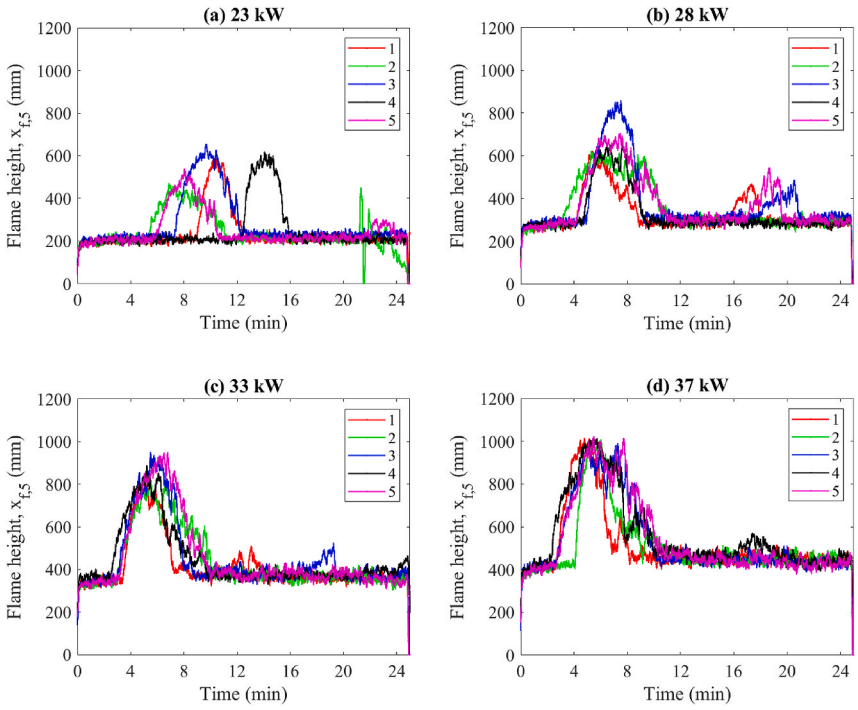

Fig. 10. Flame height ($x_{f,5}$) comparison for particle-board panels. Each graph includes all the 5 experiments (labelled 1–5) under the corresponding heat-release rate with experiment duration 25 min. The fluctuation observed (1250–1500s) for experiment 2 with 23 kW (green curve) was due to gas-flow malfunction. (For interpretation of the references to colour in this figure legend, the reader is referred to the Web version of this article.)

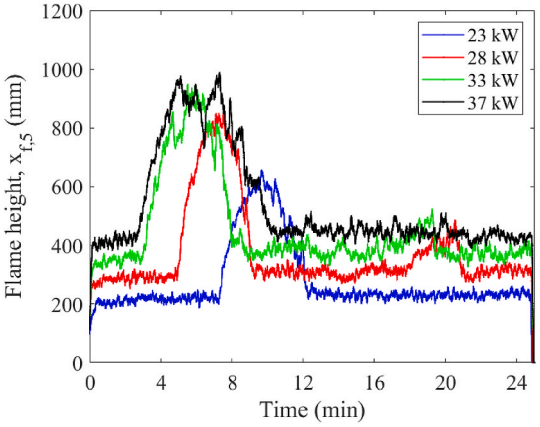

Fig. 11. Flame height ($x_{f,5}$) comparison. Variation in ignition times and peak flame heights for experiments with different heat-release rates and a duration of 25 min. Each graph represents an individual experiment.

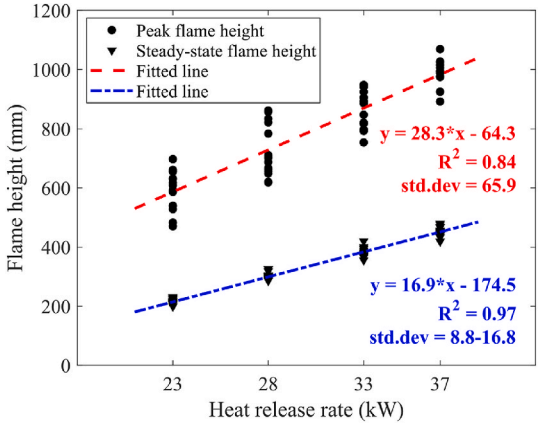

Fig. 12. Peak and steady-state flame heights for different heat-release rates. Note that the standard deviation for steady-state flame height is much less compared to that of peak flame height. Since the experiment duration does not affect the peak, only variation with heat-release rate is shown.

action. Kasymov et al. [13] reports an upward fire spread rate which varied from 0.8 ± 0.15 mm/s for chipboard to 1.38 ± 0.33 mm/s for plywood, which are much less than what is reported in this study. This difference may be due to the difference in fuel source and stability of heat released. While Kasymov et al. [13] used pine needle bulk as a fuel source, propane which has a much higher heat of combustion [39,44] was used in this study.

4.3. Charring

4.3.1. Char height, volume, area, density, and charring rate

The char height was not affected by experiment duration, as shown in Fig. 14 (a). Experimental duration was expected to impact the char height due to increased pyrolysis of the upper regions from the convective heat flow. On the contrary, it was observed that experiment duration had no significant influence on the upward progression of char in the region, within the regimes studied. However, as seen in the figure, the heat-release rate had a substantial impact on it. With every 4–5 kW increase in heat-release rate, the char height increased by 136 mm (~20%). Char height measurements had an accuracy of ±5 mm and the standard deviation varied from ~61.5 mm for 23, 28 and 33 kW, to 68.7 mm for 37 kW.

The variation in char area with experiment duration and heat-release rate is shown in Fig. 14 (b). Char area increased ~54000 mm^2 with every 4–5 kW increase in heat-release rate. There was only a slight increase in char area with experimental duration (p-value = 0.003), which is reasonable since the surface of the sample on either side of the flame are heated and pyrolyzed at a slower rate than the region directly exposed to flames. The area of the region with measurable char depth

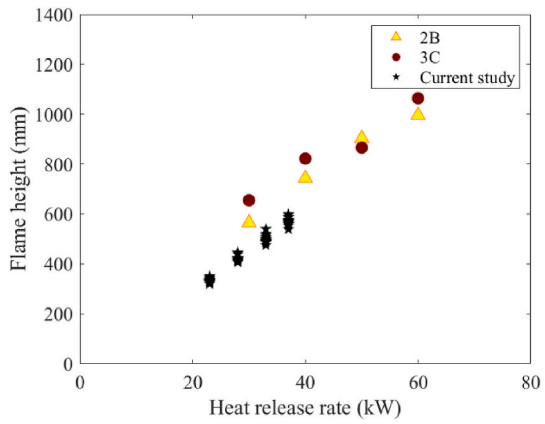

Fig. 13. Comparison of flame height measurements with the results obtained by Lee et al. [16]. Only experiments with a similar fuel location from Lee et al. has been selected for comparison. black star markers represent steady-state flame heights from this study. The other data in the legend shows two different geometries and burner locations investigated by Lee et al. [16]. The data is adjusted for difference in measurement since Lee et al. measured flame height from the neutral plane and this study measured it from the bottom of the sample.

showed a similar behaviour, as shown in Section 3.3.3. Char area measurements had an accuracy of $\pm 0.2 \times 10^4$ mm^2. The standard deviation of char area varied from 1.5 to 3.4 $\times$ 10^4 mm^2 increasing with heat-release rate.

The char volume was measured as described in Section 2.3.2 and was affected by both time and heat-release rate, as shown in Fig. 14 (c). With every 4–5 kW increase in heat-release rate, the char volume increased by $\sim 3 \times 10^5$ mm^3, and with every 5 min increase in experiment duration the char volume increased by $\sim 1.7 \times 10^5$ mm^3 on average. The char volume for 28 kW fire in 15 min is comparable with the volume for 23 kW at 25 min, and similarly for 37 kW at 15 min and 23 kW at 20 min. As explained in Section 2.3.2, char volume was not directly measured like char height or char area. Char depth was measured from nodes on a 50 mm $\times$ 50 mm grid and then the depth values of the nodes of each cell were averaged to an assumed cuboid block of volume 50 $\times$ 50 $\times$ *depth* mm^3. The resolution of measurement points and the averaging of depth at the nodes must be considered when interpreting the char volume measurements. Standard deviation of char volume varied from 0.32 to 1.9 $\times$ 10^5 mm^3. Measurement errors are small compared to this (order of 0.07 $\times$ 10^5 mm^3).

Fig. 15 shows the density of the char as obtained from the char volume and the mass reduction upon char removal. The char density is higher for lower experiment duration and lower heat-release rate. The char density was highest for 15 min experiments under 23 kW but decreased both with heat-release rate and experimental duration and seemed to approach a minimum value of ~220 kg/m^3. Schmid and Frangi [45] measured the char layer density to vary from ~220 to ~35 kg/m^3, depending on the char layer thickness. Since mass of the char removed was measured from the change in mass of the sample before and after char removal, char layer densities for individual char layer thickness could not be estimated. Therefore, the data shown in Fig. 15 is an average of densities of char layer with different thickness and undergone different stages of pyrolysis. In addition, Schmid and Frangi [45] presents the char layer densities after drying the char under 105 °C. In contrast, densities in this study will include density of some moisture as well.

In Fig. 16 visible char height (h_{ch}) and measurable char height (depth >1 mm) (h_{ch^*}) are plotted against the peak averaged flame height

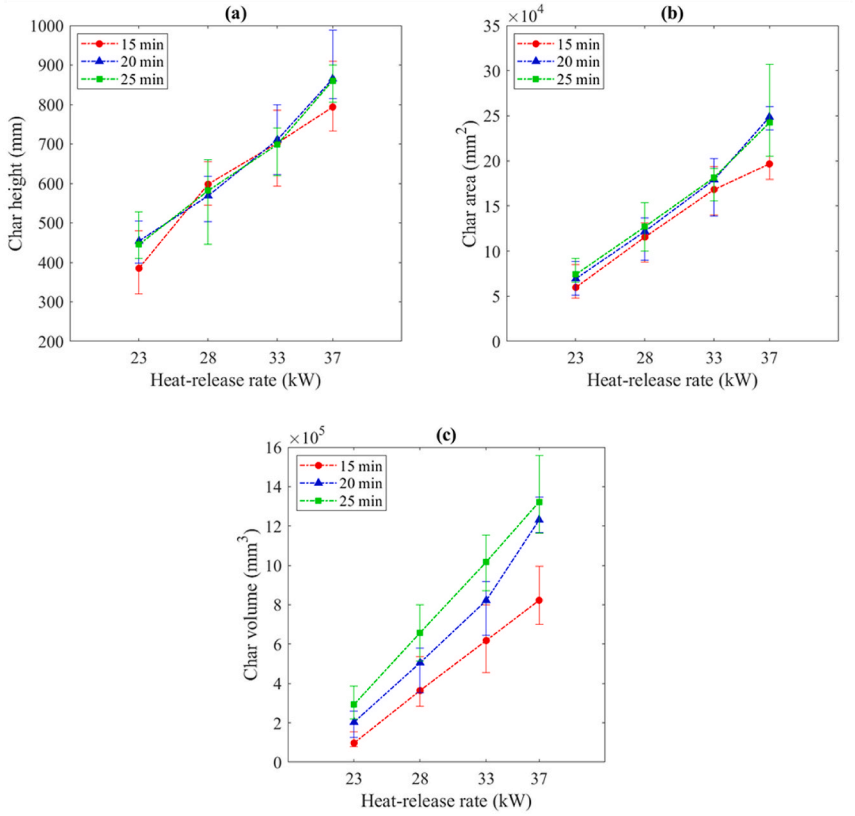

Fig. 14. Variation of (a) char height, (b) char area and (c) char volume with experiment duration and heat-release rate. The increase in experiment durations is not accompanied by any significant increment in char height or char area. Char volume is affected by both experiment duration and heat-release rates. The markers denote average values, and the error bars show range of data.

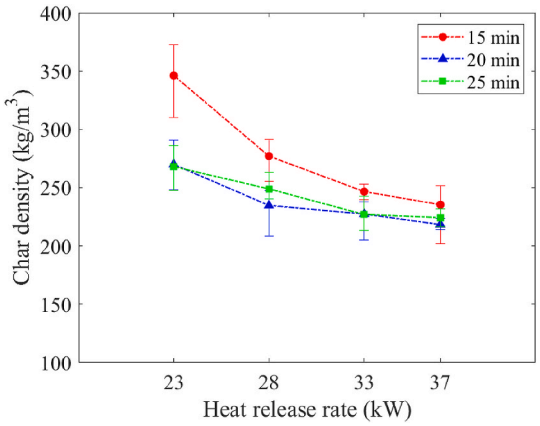

Fig. 15. Density of char removed at the end of the experiment determined from the measured char volume and mass reduction upon char removal.

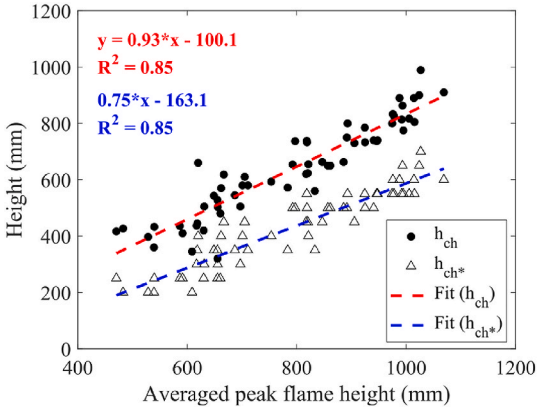

Fig. 16. Variation of visible char height (h_{ch}) and measurable char height (depth >1 mm) (h_{ch*}) with averaged peak flame height.

($x_{f,peak}$). h_{ch*} was ~66% of h_{ch}, thus these two quantities are proportional.

An approximate rate of charring was estimated at the region with highest char depth, as shown in Fig. 17, except where samples burned through. The char depth at the end of each experiment was divided by the experimental duration to produce the estimate. The charring rate increased by ~0.09 mm/min with every 4–5 kW increase in heat-release rate. The charring rate reported for higher heat-release rates were similar to that reported by Fischer [46] for densities similar to the sample in this study.

The main trend shown in Fig. 17, with a lower-than-linear increase in (local) charring rate with increasing heat-release rate, is reasonable. As the thickness of the char layer *locally* increases, heat conduction from the heated surface to the un-pyrolyzed material behind the char layer is reduced. The figure demonstrates that this is not fully compensated by the increase in heat-release rate.

Fig. 18 shows the change in average mass-loss rate with the duration of the experiment and heat-release rate. Only an average rate for the entire duration of the experiment is given here. However, the graph demonstrates that further heating after the peak did not change the mass-loss rate. As seen from Fig. 14 (a & b), and further illustrated in Section 3.3.3, increased experiment duration resulted in increased char penetration into the panel but not increased upward fire spread. Assuming most of the mass-loss happened from the region exposed to the flames (region with deeper char) and not so much from the region above h_{ch*}, there was a steady progression of charring into the panel based on the steady-state mass-loss rates. Mass-loss rates are less than what is required for ignition and sustained fire spread (1–4 g/m^{2}s [23,47]). Consistently, flames extinguished as soon as the gas flow was turned off (except for experiments with 23 kW for 15 min as explained in Section 2.3.

The quantities in Figs. 17 and 18 are closely related. The main difference between them, non-linear versus linear dependency on heat-release rate, can be understood from the fact that while Fig. 17 shows a *local* quantity, the entire sample contributes to the mass-loss rate in Fig. 18. With increasing heat-release rate, an increasing sample area contributes to the total mass loss.

4.3.2. *Temperature profile*

Temperature measurements were taken every 80 mm vertically near the surface of the sample. Thermocouples used were type K and class 1 with approximately ±10 K accuracy as stated by the manufacturer [48]. An oscillatory movement of the thermocouples, ± 10 mm, in the vertical direction was noticed during the experiments from convective flows. Due to reduced stiffness caused by heat exposure, thermocouples were in some – but not all – cases found to be displaced ~5–10 mm downwards at the end of the experiments compared with initial positions. This small variation in position is not expected to affect the result significantly. In these cases, the thermocouples were repositioned before the next experiment started. A statistical analysis of temperature data from experimental runs with identical parameters was performed, and standard deviations relative to the average temperature were approximately: 9–16% before ignition of the sample from external venting flames,

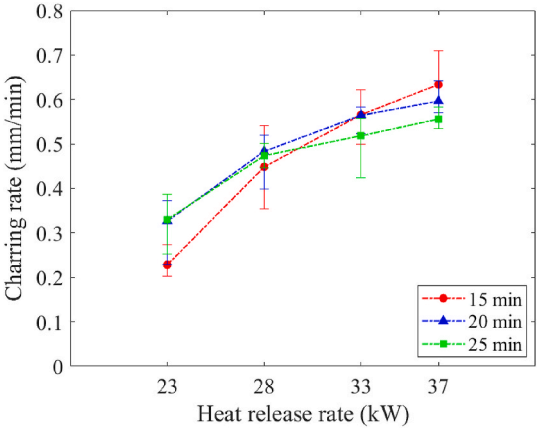

Fig. 17. Charring rate estimated in the region with highest char depth. Charring rate seems to get stable around ~0.65 mm/min which is comparable to the rate of charring for timber in literature [21,22,45].

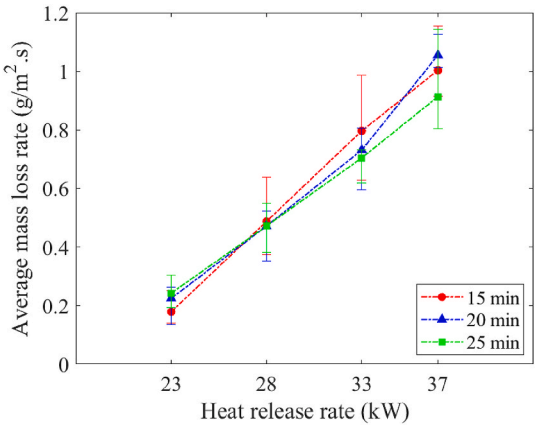

Fig. 18. Average mass-loss rate per unit area over the entire duration of the experiment. The mass-loss rate shows little variation with experiment duration but vary with the heat-release rate.

2–10% at the peak flame height phase, and 9–18% during the steady-state phase. This variation reflects both thermocouple measurement accuracy and run-to-run variations in the fire evolution.

The data was used to study the vertical temperature profile along the surface under variation in flame behaviour. Fig. 19 shows the temperature profile from (single) experiments with 20 min duration for each heat-release rate. Flame behaviour were divided into three phases: before ignition of the sample (region 1 in Fig. 7(I)), at peak flame height (Fig. 7(II)(c)), and steady-state after peak flame height (region 4 in Fig. 7 (I)). Thermocouples at 80 and 160 mm showed higher temperatures during the period leading up to ignition compared to thermocouple at 0 mm. Ignition of the samples during the experiment usually occurred between 80 and 160 mm from the bottom, since this was the point where the external venting flames first contacted the sample after being ejected from the fire compartment. Once ignited, the flames spread to lower part of the sample, increasing the temperature at 0 mm. Fig. 19 shows that the temperatures at lower heights during the steady-state flaming phase increase more with heat-release rate compared with temperatures before ignition of the samples. This could be a result of char oxidation of the samples in the steady-state phase in addition to the contribution of flames emerging from the compartment. As shown in Fig. 19, for inert panels the thermocouple at 80 mm recorded the highest temperature followed by a steady reduction with height. The temperature at the top of the inert sample displayed only slight variations with heat-release rate, while the values measured at 80 mm had a 500 °C increase between 23 kW and 37 kW. The samples show a relatively similar trend in thermal profile between flaming phases except during the peak flame height. This may be due to higher variations in the flame behaviour during the peak. The vertical temperature profiles for inert samples are comparable to the results reported by Lu et al. [49] and Tang et al. [50].

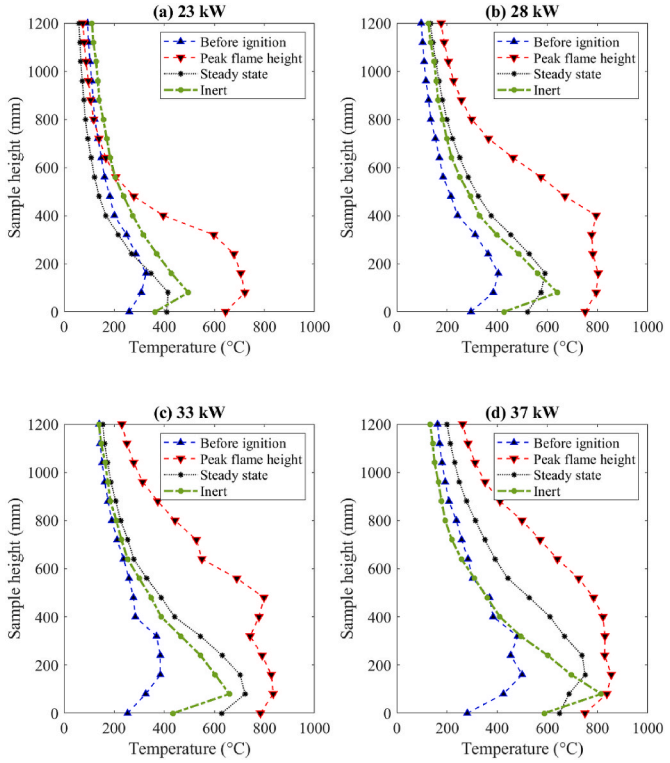

Fig. 19. Vertical temperature profile (horizontal axis) for 20 min experiments for the three flaming phases; before ignition, at the peak and during steady-state burning (see main text and Fig. 7) along the height of the sample surface above the lower edge of the board (vertical axis). Each curve shows an average of a series of temperatures measured at different stages of the same experiment. The temperature profile for inert samples under corresponding heat-release rates are included for comparison.

In Fig. 20, temperatures at a few measurement points are compared with the evolution of the flame height. Note that the heights for these measurements are *not* the same for the various heat-release rates but selected relative to the steady-state and peak flame heights (both of which increase with heat-release rate). In all cases there is a clear – but unsystematic – influence on the temperatures from the flame peak. The temperature evolution in Fig. 20 is comparable to that reported by Koutaïba et al. [14] for timber panels.

4.3.3. Char depth variation with heat-release rate and experiment duration

The char depth was affected by both experiment durations and heat-release rate, as demonstrated in Fig. 21 and Fig. 22. The figures are constructed as a superposition of contour plots of the char depth (after removal of char) and the visual cracking pattern (before char removal). Fig. 21 shows how char depth varied with heat-release rate for 25 min experiments and Fig. 22 shows how experiment duration influenced char depth for 37 kW experiments. Char depth was observed to increase with both heat-release rate and experiment duration. However, the height to which char depth could be measured (height of the contour) did not increase significantly with experiment duration (Fig. 22) but increased with heat-release rate (Fig. 21). In many of the 25 min experiments, the panel burned through at the bottom. The charring patterns were tilted to the right side in most cases, most likely due to the airflow conditions in the lab.

The influence of both experiment duration and heat-release rate will be displayed in a more condensed way. To reduce the values from the char depth matrix of each sample to a column, thereby avoiding influence from shape (like tilt) as well as reducing other measurement errors, the average of each row of perforations on the grid (as shown in Fig. 5) were calculated (Fig. 23). For each experiment, this leads to a column of average depth values, which will be referred to as an averaged column.

The mean of all the averaged columns from experiments with the same parameters was then used to create the graphs shown in Fig. 24. Each line is therefore an average char depth for 5 experiments.

Fig. 24 clearly shows that the average char depth (d_{avg}) increases over time, but that h_{ch^*}does not vary significantly with experimental duration. The average char depth increases with experiment duration while h_{ch^*} remains the same unless the heat-release rate is increased. Standard deviation of the char depth between individual experiments is up to 1 mm, increasing with heat-release rate and duration and decreasing with height. Koutaïba et al. [14] shows a similar trend in char depth variation with height. Koutaïba et al. measures char layer thickness at individual locations along the height of the sample, compared to twice-averaged values shown in Fig. 24.

In Fig. 24, an increase in the average char depth (d_{avg}) when the experiment duration increased from 15 to 20 min for each heat-release rate may be noted. Although there is a significant increase between 20 and 25 min as well, it is less compared to the increase between 15 and 20 min. To explore this behaviour, the thermal penetration time for the sample was calculated to be ~925 s. With increased experiment duration, the heat front reaches the back of the sample and moves more slowly into the inert back panel (compare thermal conductivity values in Table 1). Further heating would increase the internal temperature of the sample rapidly as heat loss by conduction decreased. This could explain the significant increase in char depth when experiment duration exceeded 15 min (900 s).

5. Discussion

5.1. Flame heights

This study investigates the flame and char behaviour under varying heat-release rates and experimental duration, and how it affects the fire spread. The intermittent flamelets will also contribute to heat transfer into the sample and eventually pyrolyze it. In addition, the connected flame height being much smaller than the averaged flame height

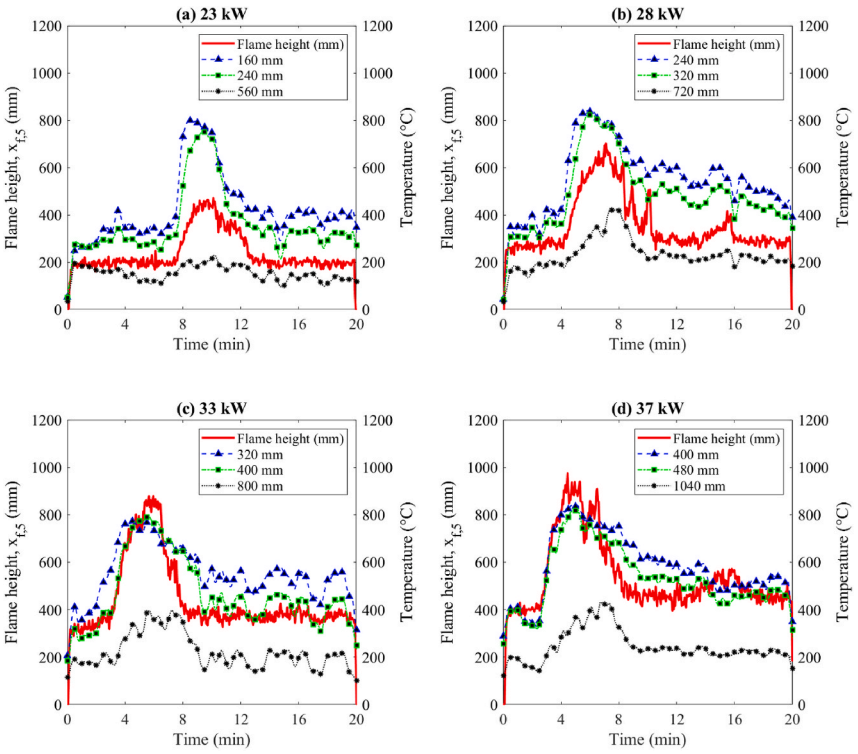

Fig. 20. Flame heights and temperature evolution below the steady-state flame height (blue), just above the steady-state (green) and above the peak flame height (black). Temperature data was smoothened with a 24 s moving average and flame heights were averaged every 3 s to match the data collection interval of thermocouples. (For interpretation of the references to colour in this figure legend, the reader is referred to the Web version of this article.)

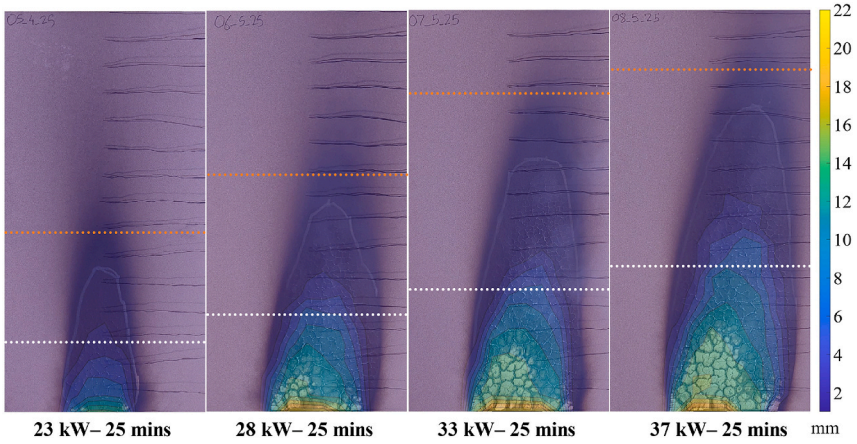

Fig. 21. Influence of heat-release rate on the charring depth on particle board samples. The orange line in the image is the peak flame height for that experiment and the white line is the plateau flame height. (For interpretation of the references to colour in this figure legend, the reader is referred to the Web version of this article.)

including flamelets, could also lead to underestimation of the fire spread. Therefore, flame heights in this study were estimated from the highest points of luminous combustion.

Consalvi et al. [18] show how inconsistent definitions of flame height can generate differences in perceived wall heat flux of the order of 50%. Consalvi et al. also state that since it is the heat flux incident on the combustible surface that drives fire spread, it is reasonable to define flame height as a quantifiable heat-flux threshold (height at which the incident heat flux on the sample surface exceeds a threshold value). However, to measure the heat-flux profile across the height of the sample directly, holes must be drilled into the sample, which could compromise the charring behaviour of the surface.

Fig. 25 illustrates the differences in flame heights obtained from the three different methods discussed above. The green curve represents the method used in this study, while red represents the connected flames (excluding flamelets as described in Sjöström et al. [17]) for the same experiment. For 50% intermittency, represented by a blue curve, every 120 frames (5 s) were considered to find the height to which flames were present 50% of the time. Estimation of flame height with the flamelets included shows ~50% higher values during the peak flaming period compared with the other two methods. In the steady-state period, the measurement with flamelets showed ~46% (137 mm) increase and those with connected flames showed ~23% (70 mm) increase compared with intermittent flame height measurements. Fig. 25 also shows the corresponding values of visible char height(h_{ch}) and measurable char height (depth >1 mm) (h_{ch^*}) for that experiment. h_{ch^*} is close to the peak flame height values measured using continuous and 50% intermittency methods, while h_{ch} is higher than those two peak values. Saito et al. [11]

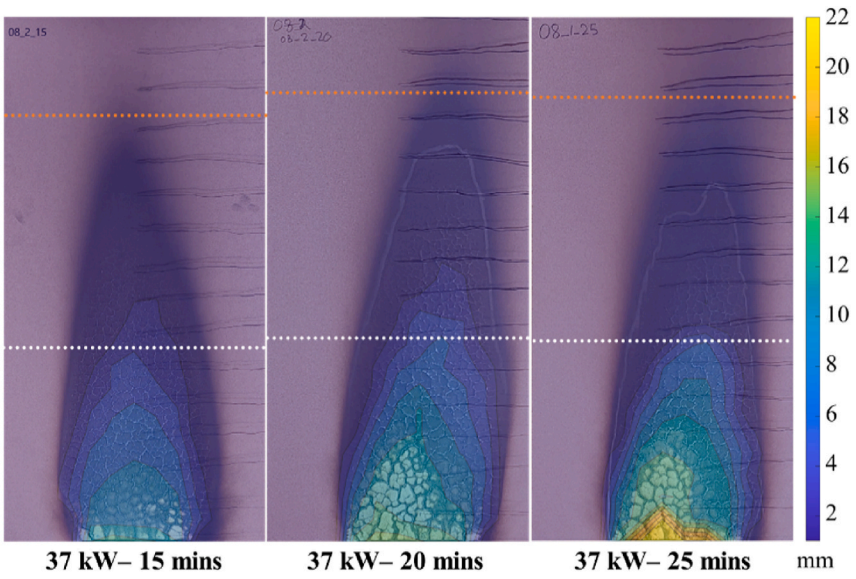

Fig. 22. Variation in charring depth on particle board samples with experiment duration. The orange line in the image is the peak flame height for that experiment and the white line is the plateau flame height. (For interpretation of the references to colour in this figure legend, the reader is referred to the Web version of this article.)

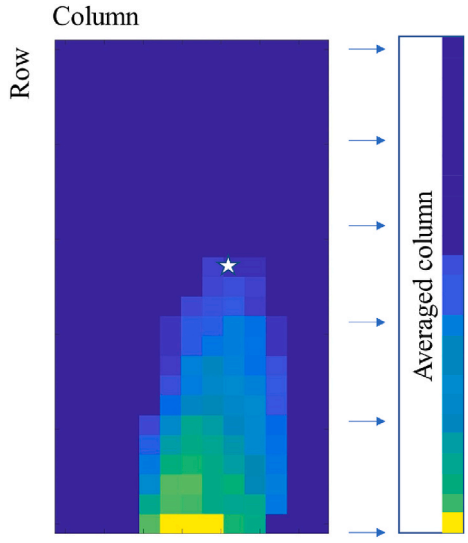

Fig. 23. Averaging depth cells. Each cell represents a depth measurement from a node in the grid panel. The point marked by the star is the highest point on the panel where depth could be measured, h_{ch^*}.

states that upward fire spread occurs due to heat transfer to the fuel in the region above the pyrolyzed region. In other words, upward flame spread occurs when the flame height is higher than the pyrolysis height. Considering h_{ch} as the extent of pyrolysis, the definition of flame height used in this study (green curve) predicts further vertical flame spread to occur, inconsistently with the result. However, peaks of both continuous and 50% intermittent flame heights being lower than h_{ch}, correctly predicts the absence of fire spread.

Fig. 26 shows the temperature profiles for an experiment with heat-release rate 33 kW measured by the thermocouples 1–2 cm from the surface of the sample. The profile shown for inert panel is from the same interval (at an earlier stage in the experiment compared to Fig. 19), 1 min–3 min after the flames emerge from the compartment, as the profile before ignition of the particle board panel. As stated in Section 3.2, the surface of the inert material is indeed at a higher temperature compared with the particle board before ignition. At lower heights, the temperature after the peak for the particle board is higher than that of the inert panels. The temperature gradually reduces with height and becomes less than for the inert panel above 320 mm. The steady flame heights for that experiment after the peak was also ~300 mm. The reduction in temperature for the particle board above 320 mm could be due to increased thermal conduction into the sample compared to inert panel. A tendency for slightly higher flame heights can be discerned in Fig. 9 for the particle board panel during the steady-state. This is probably due to some production of pyrolysis gases.

When the gas burner was switched off, the flames on the panels self-extinguished as well, except for the series of experiments with 23 kW for 15 min. For those experiments there were flames on the panel even after the gas was turned off, probably since the ignition happened near the termination of the experiments. As flames from propane were present for just sufficient time to cause ignition of the sample but not to exhaust all the pyrolysis gases, the samples continued burning. These flames were extinguished immediately after.

5.2. Charring and fire spread

The charring and fire spread along the sample due to external venting flames are discussed in this section. Flames emerging from the compartment onto the particle board raise its surface temperature leading to thermal decomposition. It may be assumed that the particle boards in this study have similar thermal decomposition behaviour as timber. Dehydration of the sample along with very slow pyrolysis occur from 100 °C to 200 °C, onset of rapid pyrolysis up to 300 °C and rapid pyrolysis above 300 °C [8,21,51]. Charring is assumed to occur at 300 °C [8], which is different from pyrolysis where chemical decomposition may start without surface deformation. As the exposed region undergoes pyrolysis and the mass-loss rate becomes high enough for production of a suitable gaseous mixture, flames from the compartment ignite it. This increased flaming transfers more heat to the region immediately above the already ignited region. The region above has already been preheated by the flames and hot gases and starts pyrolyzing, but with a mass-loss rate insufficient to cause ignition. Ignition of the sample provide that additional heat flux required for the preheated region to pass the critical mass-loss rate for ignition (~1–3 g/m^{2}s for timber [47]) and the flame to spread upwards. Since changes in mass-loss over time could not be measured during the experiment, the mass-loss rate during ignition

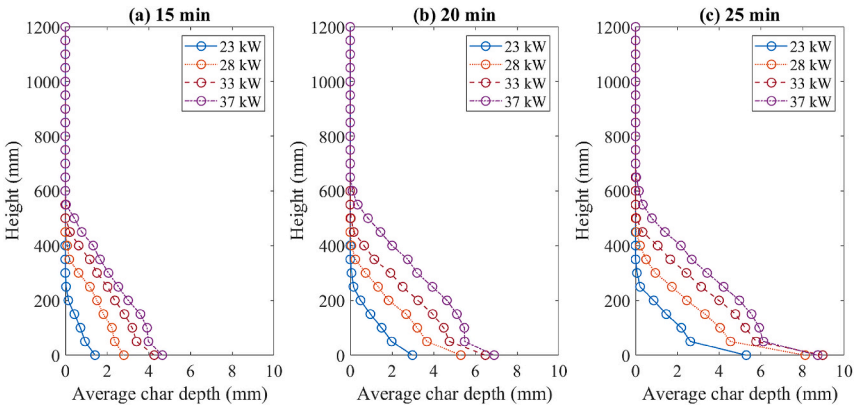

Fig. 24. Variation in average depth with heat-release rate for different experiment durations. The depths are averaged across the width of the panel and averaged again over the five experiments with identical experimental duration and heat-release rate. Note that the range of the vertical axis corresponds to the height of the particle board.

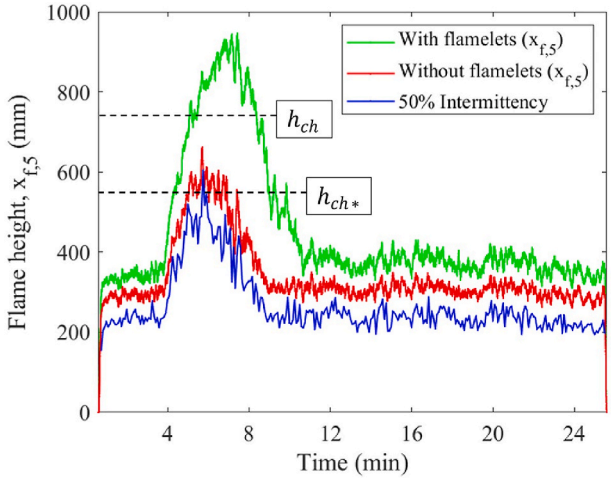

Fig. 25. Flame height comparison based on three different definitions. Flame height including the flamelets as used in this study (green curve), continuous flames excluding flamelets (red curve) and flame height with 50% intermittency for every 5 s (blue curve) are shown. h_{ch} and h_{ch*} for the corresponding experiment are also indicated. (For interpretation of the references to colour in this figure legend, the reader is referred to the Web version of this article.)

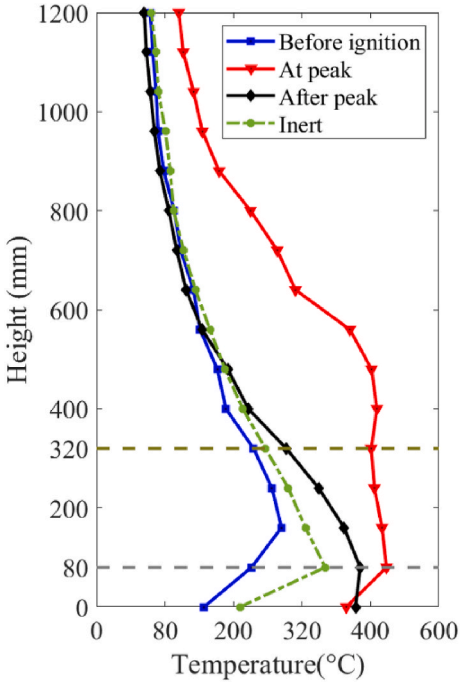

Fig. 26. Vertical temperature profiles are shown for an experiment on particle board with total heat-release rate 33 kW – before ignition of the sample from external venting flames, during peak flame height, and after the peak in flame height when the flame height returns to steady-state (see Section 3.3.2 and Fig. 7). A temperature profile for an experiment on an inert panel at 33 kW is shown for comparison. The temperature for the inert sample at 80 mm is ~670 °C while for the particle board before ignition, it was ~460 °C.

could not be determined. The convective heat flux may also contribute to the charring.

Starting from the initially ignited lower layers of the sample, the char formed typically prevents heat transfer into the unaffected fuel layer, lowering pyrolysis gas production [52]. Reduction in pyrolysis-gas production reduces the flaming combustion, and as a result the heat flux incident on the region above the already charred sample surface is reduced, which in turn prevents pyrolysis of the sample further above. The flame height achieves a peak value, and as the char layer develops, the flame height is reduced (see Fig. 7 (I)), as also observed in previous studies [11,12]. Continued presence of flames from the fire compartment would degrade the exposed surface region further, leading to cracking and shrinking of the char, with fresh wood layers exposed [53]. This may be responsible for the smaller secondary peaks in the flame height profile, as shown in Fig. 10.

The peak flame height increased only with heat-release rate and not with experiment duration. Once the flame height decreased to steady levels after the peak, further exposure did not result in increased char height or further upward fire spread, as shown in Fig. 14 (a). However, increased experiment duration caused deeper char layers and increased char volumes, as shown in Fig. 14 (c). The charred area (a_{ch}) was not affected by increased experiment duration, as shown in Fig. 14 (b). Without the presence of the flames, the upper regions were only exposed to hot-gas flows, which heated the sample but not enough to cause adequate pyrolysis for continued flame spread.

Buchanan and Abu [21] state that the density of wood drops to 20% of its original value when converted to char as temperature exceeds 300 °C. The density of char as measured in this study varied between 31% and 49% of the original density. As shown in Fig. 15, the density was higher for lower heat-release rates and lower experiment durations. To summarize, with no increment in char height or area, it was the char depth and in turn the volume that increased with experiment duration. In addition, increased experiment duration and heat-release rate resulted in reduced char density. Thus, charring of the sample limits upward

flame spread as the pyrolysis gases available for combustion is reduced. However, continued exposure to flames will lead to further heat conduction inwards, creating deeper char layers in the already charred region.

It may be assumed that the region of the surface with highest temperature as reflected by the thermocouple data in Fig. 19, will ignite first. Based on the temperature measurements in all the experiments, the highest recorded temperatures were between 80 and 160 mm from the bottom of the panel. The high temperature at a higher location rather than at the bottom is assumed to be caused by the momentum of the flames as they were ejected out of the combustion chamber; keeping the flames away from the bottom of the panel and the thermocouple located there. It was this higher region that ignited first, and it was expected that this area should have highest char depth as it had been exposed to relatively higher temperatures. A significant increase in char depth in this region is not evident in the data. The deepest char is observed at the bottom of the panel and not ~80–160 mm above the bottom. This may be due to air flow towards the fire through the gap between the bottom of the panel and roof of the compartment supplying more oxygen to the combustion zone or it may be due to the large separation between measurement points (50 mm). It may also be due to heat accumulation at the bottom of the sample from reduced net conductive heat loss from this region due to geometric constraints (reduction in amount of material available for conduction).

5.2.1. Relevance for full-size buildings

The current study had an opening factor (as defined in Drysdale [54]) of 0.07 $m^{1/2}$ and reported stable average flame heights of ~200 mm, ~286 mm, ~360 mm and ~435 mm (after peak) for heat-release rates of 23 kW, 28 kW, 33 kW and 37 kW, respectively. Height of external venting flames on a facade in a full-scale scenario was investigated by Sjöström et al. [17]. Sjöström et al. used realistic furniture as the fuel source to simulate a real fire scenario and had an opening factor of 0.062 $m^{1/2}$ for their study and reported an average flame height around ~3500 mm–4000 mm. Oleszkiewicz [55] measured heat flux density in a full-scale experimental setup using propane gas as the fuel source with an opening factor of 0.057 $m^{1/2}$. Heat-release rates in the experiments by Oleszkiewicz varied from 5.5 MW to 10.3 MW and measured heat fluxes from 19.2 kW/m^2 – 68.3 kW/m^2 at heights as low as 500 mm above the ventilation opening. However, the heat fluxes at 2500 mm were in the interval 3.5 kW/m^2 – 13.7 kW/m^2 as heat-release rate was varied. Heat flux incident on the façade significantly reduced with an increase in height of only 1000 mm even for a full-scale fire scenario, similar to the results presented in this study. However, since heat flux was not measured in this study, a direct comparison is not possible.

The height of an external venting flame from a compartment under post-flashover conditions depends on the rate of burning of the fuel and dimensions of the ventilation opening [56]. Since these data are presented in the study, the results can contribute to numerical modelling of fire spread on timber façades and can assist in a sustainable and safe timber-based built environment. Data for peak flame height may be used to predict what is the typical height between windows of two consecutive floors to minimize fire spread based on the expected maximum heat-release rate from the fire compartment. The data about char formation could help to understand the progression of char into the façade and in turn, the stability of the façade, as a function of exposure time and heat-release rate. In addition, the data could be used to design façade support structures and external fire breaks on a timber façade. The study also explores how the external venting flame height can change when an existing inert façade is replaced with a charring timber-based façade and the data can be useful in fire safety design of a building renovated with timber-based façade instead of an existing inert façade.

6. Conclusion

A series of small-scale experiments were conducted to study the fire spread and charring on a vertical particle board panel under varying heat-release rate in the fire compartment and experimental duration. A peak flaming period was observed, with steady burning periods before and after the peak. Experiment duration did not influence upward flame spread after the peak when no additional external heat flux was provided. An average fire-spread rate of ~3.2 mm/s and decay rate of ~2.5 mm/s were estimated for the peaks. Char behaviour under varying flame heights and experiment durations were quantified. With every 4–5 kW increase in heat-release rate, char height increased by ~136 mm, char volume by ~3 × 105 mm^3 and char area by ~540 cm^2. Char height and area showed negligible influence from experiment duration but with every 5 min increase the char volume increased by ~1.7 × 105 mm^3. Interestingly, the char density did not decrease linearly with increasing heat-release rate but seemed to stabilise around 220 kg/m^3. A linear increase in mass-loss rate was observed with increasing heat-release rate. The measurable char height (depth >1 mm) (h_{ch^*}) was ~60–70% of the visible char height (h_{ch}) when plotted as functions of peak flame height. Variations in average char depth along the height of the panel with heat-release rate and experiment duration were also quantified. While the fire did not spread upwards with increased experiment duration, deeper char layers were created.

Further experiments with a broader range of heat-release rates and experiment durations may be necessary to understand the changes with increased scale. It is also recommended to explore how the presence of the window head affects the results. Direct measurement and investigation of mass-loss rate, heat flux on the sample surface and heat-release rates is also recommended as future work. A further study may also include proper control over the moisture of the sample and char measurements using photogrammetry. Change in flame height and flame spread behaviour for a double-layered façade with a cavity (ventilation cavity) would also be of interest, since this is a common construction method for timber façades.

Funding

This work was supported by The Research Council of Norway, Project 301569: Building Design for At-risk Groups (BUILDER).

Author statement

Dheeraj Dilip Karyaparambil: Methodology, Software, Formal analysis, Investigation, Data Curation, Writing - Original Draft, Visualization.

Sveinung Erland: Formal analysis, Writing - Original Draft, Writing - Review & Editing, Supervision.

Patrick van Hees: Writing - Original Draft, Writing - Review & Editing, Supervision.

Vidar Frette: Conceptualization, Writing - Original Draft, Writing - Review & Editing, Supervision, Project administration, Funding acquisition.

Bjarne Christian Hagen: Conceptualization, Writing - Original Draft, Writing - Review & Editing, Supervision, Funding acquisition.

Guideline: https://www.elsevier.com/authors/policies-and-guidelines/credit-author-statement.

Declaration of competing interest

The authors declare that they have no known competing financial interests or personal relationships that could have appeared to influence the work reported in this paper.

Data availability

Data will be made available on request.

Acknowledgements

The authors would like to thank the Western Norway University of Applied Sciences, Lund University, and the University of Bergen for their support.

References

[1] L. Makovicka Osvaldova, Introduction, in: Wooden Façades Fire Saf. Eff. Jt. Type Ignition Behav., Springer International Publishing, Cham, 2020, pp. 1–23, https://doi.org/10.1007/978-3-030-48883-3_1.
[2] Twenty Per Cent of New Homes in Amsterdam to Be Constructed from Timber, Dezeen, 2021. https://www.dezeen.com/2021/11/02/amsterdam-new-buildings-20-per-cent-timber/. (Accessed 18 November 2021).
[3] Top 5 tallest timber buildings in the world, Constr. Rev. Online. (2021). https://constructionreviewonline.com/biggest-projects/top-5-tallest-timber-buildings-in-the-world/. (Accessed 18 November 2021).
[4] R. Abrahamsen, Mjøstårnet-Construction of an 81 M Tall Timber Building, Int. Holzbau-Forum IHF, 2017, p. 13. https://www.moelven.com/globalassets/moelven-limtre/mjostarnet/mjostarnet—18-storey-timber-building-completed.pdf. (Accessed 19 May 2020).
[5] M. Bonner, G. Rein, List of facade fires 1990 - 2020, build, Environ. Zenodo. 169 (2020), https://doi.org/10.5281/zenodo.3743863, 10654–0.
[6] BBC News, Grenfell Tower: what Happened, BBC News, 2019. https://www.bbc.com/news/uk-40301289. (Accessed 19 December 2021).
[7] C. Carlson, Milan Apartment Block Fire "Closely Recalled Grenfell Tower" Says Mayor, Dezeen, 2021. https://www.dezeen.com/2021/08/31/milan-apartment-block-fire-torre-del-moro-grenfell/. (Accessed 19 December 2021).
[8] A.I. Bartlett, R.M. Hadden, L.A. Bisby, A review of factors affecting the burning behaviour of wood for application to tall timber construction, Fire Technol. 55 (2019) 1–49, https://doi.org/10.1007/s10694-018-0787-y.
[9] E.K. Asimakopoulou, K. Chotzoglou, D.I. Kolaitis, M.A. Founti, Characteristics of externally venting flames and their effect on the façade: a detailed experimental study, Fire Technol. 52 (2016) 2043–2069, https://doi.org/10.1007/s10694-016-0575-5.
[10] X. Sun, L. Hu, X. Zhang, Y. Yang, F. Ren, X. Fang, K. Wang, H. Lu, Temperature evolution and external flame height through the opening of fire compartment: scale effect on heat/mass transfer and revisited models, Int. J. Therm. Sci. 164 (2021), 106849, https://doi.org/10.1016/j.ijthermalsci.2021.106849.
[11] K. Saito, J.G. Quintiere, F.A. Williams, Upward turbulent flame spread, 75–86, https://doi.org/10.3801/iafss.fss.1-75, 1986.
[12] E.G. Brehob, A.K. Kulkarni, Experimental measurements of upward flame spread on a vertical wall with external radiation, Fire Saf. J. 31 (1998) 181–200, https://doi.org/10.1016/S0379-7112(98)00012-5.
[13] D. Kasymov, M. Agafontsev, P. Martynov, V. Perminov, V. Reyno, E. Golubnichiy, Thermography of wood-base panels during fire tests in laboratory and field conditions, in: L. Makovicka Osvaldova, F. Markert, S.L. Zelinka (Eds.), Wood Fire Saf., Springer International Publishing, Cham, 2020, pp. 203–209, https://doi.org/10.1007/978-3-030-41235-7_31.
[14] E.M. Koutaïba, D. Dhima, M. Duny, J.P. Garo, H.Y. Wang, Q. Jullien, Experimental study on vertical wooden façade combustion, Procedia Eng. 210 (2017) 520–527, https://doi.org/10.1016/j.proeng.2017.11.109.
[15] E.E. Zukoski, B.M. Cetegen, T. Kubota, Visible structure of buoyant diffusion flames, Symp. Combust. 20 (1985) 361–366, https://doi.org/10.1016/S0082-0784(85)80522-1.
[16] Y.P. Lee, M.A. Delichatsios, G.W.H. Silcock, Heat fluxes and flame heights in façades from fires in enclosures of varying geometry, Proc. Combust. Inst. 31 II (2007) 2521–2528, https://doi.org/10.1016/j.proci.2006.08.033.
[17] J. Sjöström, D. Brandon, A. Temple, E. Hallberg, F. Kahl, D. Brandon, E. Hallberg, F. Kahl, A. Temple, J. Sjöström, D. Brandon, A. Temple, Exposure from Mass Timber Compartment Fires to Facades, RISE Research Institutes of Sweden, Fire Technology, Safety and Transport, RISE Research Institutes of Sweden, 2021. http://ri.diva-portal.org/smash/get/diva2:1594601/FULLTEXT01.pdf.
[18] J.L. Consalvi, Y. Pizzo, B. Porterie, J.L. Torero, On the flame height definition for upward flame spread, Fire Saf. J. 42 (2007) 384–392, https://doi.org/10.1016/j.firesaf.2006.12.008.
[19] L. Hu, Z. Qiu, K. Lu, F. Tang, Window ejected flame width and depth evolution along facade from under-ventilated enclosure fires, Fire Saf. J. 76 (2015) 44–53, https://doi.org/10.1016/j.firesaf.2015.05.001.
[20] E.K. Asimakopoulou, D.I. Kolaitis, M.A. Founti, Geometrical characteristics of externally venting flames: assessment of fire engineering design correlations using medium-scale compartment-façade fire tests, J. Loss Prev. Process. Ind. 44 (2016) 780–790, https://doi.org/10.1016/j.jlp.2016.09.006.
[21] A.H. Buchanan, A.K. Abu, Timber structures, in: Struct. Des. Fire Saf., second ed., 2017, pp. 257–300, https://doi.org/10.1002/9781118700402.ch9.
[22] K.L. Friquin, Material properties and external factors influencing the charring rate of solid wood and glue-laminated timber, Fire Mater. 35 (2011) 303–327, https://doi.org/10.1002/fam.1055.
[23] R. Emberley, A. Inghelbrecht, Z. Yu, J.L. Torero, Self-extinction of timber, Proc. Combust. Inst. 36 (2017) 3055–3062, https://doi.org/10.1016/j.proci.2016.07.077.
[24] Q. Xu, L. Chen, K.A. Harries, F. Zhang, Q. Liu, J. Feng, Combustion and charring properties of five common constructional wood species from cone calorimeter tests, Construct. Build. Mater. 96 (2015) 416–427, https://doi.org/10.1016/j.conbuildmat.2015.08.062.
[25] E.K. Asimakopoulou, K.E. Chotzoglou, D. Kolaitis, J. Zhang, M.A. Delichatsios, Experimental and numerical investigation of externally venting flame developing in a corridor-façade configuration, in: FSF 2019 – 3nd Int. Symp. Fire Saf. Facades Paris, Fr. Sept. 26-27, 2019, 2019, https://doi.org/10.1016/j.firesaf.2019.102912.
[26] B. Östman, L. Tsantaridis, Fire scenarios for multi-storey façades with emphasis on full-scale testing of wooden façades, Fire Technol. 51 (2015) 1495–1510, https://doi.org/10.1007/s10694-015-0508-8.
[27] T. Hakkarainen, T. Oksanen, Fire safety assessment of wooden facades, Fire Mater. 26 (2002) 7–27, https://doi.org/10.1002/fam.780.
[28] D. Brandon, Collection of Façade Fire Tests Including Timber Structures, Fire Technology, Safety and Transport, RISE Research Institutes of Sweden, 2020. http://ri.diva-portal.org/smash/get/diva2:1431565/FULLTEXT02.pdf.
[29] P.H. Thomas, A.J.M. Heselden, Fully developed fires in single compartments. A cooperative programme of the Conceil International du Batiment. (CIB Report No. 20), Fire Research Station Borehamwood, 1972.
[30] A.S. Würth Norge, Product data sheet - silikat dytteremse, n.d. https://nettbutikk.wuerth.no/kjemi-2/branntetting/dytteremse-silikat. (Accessed 20 December 2021).
[31] V. Babrauskas, W.J. Parker, Ignitability measurements with the cone calorimeter, Fire Mater. 11 (1987) 31–43, https://doi.org/10.1002/fam.810110103.
[32] G. Merryweather, M.J. Spearpoint, Ignition of New Zealand wood products in the LIFT, RIFT and ISO 5657 apparatus using the ASTM e 1321-97 protocol, J. Fire Sci. 26 (2008) 63–88, https://doi.org/10.1177/0734904107085381.
[33] G. Merryweather, M.J. Spearpoint, Flame spread measurements on wood products using the ASTM E 1321 LIFT apparatus and a reduced scale adaptation of the cone calorimeter, Fire Mater. 34 (2010) 109–136, https://doi.org/10.1002/fam.1001.
[34] A.S. Forestia, Product data sheet - forestia flooring P6. https://forestia.com/media/3099/pds_04-2020-forestia-flooring-standard-p6.pdf, 2020. (Accessed 18 January 2022).
[35] Ł. Czajkowski, W. Olek, J. Weres, R. Guzenda, Thermal properties of wood-based panels: specific heat determination, Wood Sci. Technol. 50 (2016) 537–545, https://doi.org/10.1007/s00226-016-0803-7.
[36] Skamol Group, Product data sheet - skamo enclosure board. https://www.skamol.com/download-centre/type-of-system/skamoenclosure-building, 2021. (Accessed 9 March 2022).
[37] Ytong Massivblokk Ytong, Tech. Data (2020). https://www.ytongsiporex.no/1171.php. (Accessed 16 June 2022).
[38] L. Zhang, Y. Yang, H. Zhang, G. Liu, Analysis of thermal insulation performance of aerated concrete block wall in solar greenhouse, IOP Conf. Ser. Earth Environ. Sci. 170 (2018), 32078, https://doi.org/10.1088/1755-1315/170/3/032078.
[39] D. Drysdale, Fire science and combustion, an introd. To fire dyn, 1–34, https://doi.org/10.1002/9781119975465.ch1, 2011.
[40] N. Otsu, A threshold selection method from gray-level histograms, IEEE Trans. Syst. Man. Cybern. 9 (1979) 62–66, https://doi.org/10.1109/TSMC.1979.4310076.
[41] F. Tang, P. Hu, Q. He, J. Zhang, J. Wen, Effect of sidewall on the flame extension characteristics beneath a ceiling induced by carriage fire in a channel, Combust. Flame 223 (2021) 202–215, https://doi.org/10.1016/j.combustflame.2020.09.020.
[42] T.B. Maynard, J.W. Butta, A physical model for flame height intermittency, Fire Technol. 54 (2018) 135–161, https://doi.org/10.1007/s10694-017-0678-7.
[43] M. Kokkala, D. Baroudi, W. Parker, Upward flame spread on wooden surface products: experiments and numerical modelling, Fire Saf. Sci. 5 (1997) 309–320, https://doi.org/10.3801/iafss.fss.5-309.
[44] E.T. Howard, Heat of combustion of various southern pine materials, Wood Sci. 5 (1971) 194–197. http://www.srs.fs.usda.gov/pubs/24165.
[45] J. Schmid, A. Frangi, Structural timber in compartment fires – the timber charring and heat storage model, Open Eng. 11 (2021) 435–452, https://doi.org/10.1515/eng-2021-0043.
[46] N. Fischer, S. Treml, Abbrandgeschwindigkeit von Holz und Holzwerkstoffen in Abhängigkeit von der Rohdichte, der Spangröße und der Ausrichtung der Späne, Eur. J. Wood Wood Prod. 70 (2012) 327–335, https://doi.org/10.1007/s00107-011-0565-8.
[47] S. McAllister, M. Finney, J. Cohen, Critical mass flux for flaming ignition of wood as a function of external radiant heat flux and moisture content, in: 7th US Natl. Tech. Meet. Combust. Inst., Georgia Institute of Technology, Atlanta, GA, 2011, pp. 1698–1704. https://www.fs.fed.us/rm/pubs_other/rmrs_2011_mcallister_s001.pdf.
[48] RS Components, Thermocouple selection guide. https://docs.rs-online.com/96d5/0900766b815e5302.pdf, 2022. (Accessed 23 August 2022).
[49] K.H. Lu, J. Wang, L.H. Hu, Vertical temperature profile of fire-induced facade thermal plume ejected from a fire compartment window with two adjacent side walls, Appl. Therm. Eng. 113 (2017) 70–78, https://doi.org/10.1016/j.applthermaleng.2016.11.018.
[50] F. Tang, L.H. Hu, M.A. Delichatsios, K.H. Lu, W. Zhu, Experimental study on flame height and temperature profile of buoyant window spill plume from an under-ventilated compartment fire, Int. J. Heat Mass Tran. 55 (2012) 93–101, https://doi.org/10.1016/j.ijheatmasstransfer.2011.08.045.

[51] Forest Products Laboratory, Theories of the combustion of wood and its control, Report 2136, Wisconsin, https://ir.library.oregonstate.edu/downloads/3r0%0A74z89g, 1958.
[52] D. Morrisset, R.M. Hadden, A.I. Bartlett, A. Law, R. Emberley, Time dependent contribution of char oxidation and flame heat feedback on the mass loss rate of timber, Fire Saf. J. 120 (2020), 103058, https://doi.org/10.1016/j.firesaf.2020.103058.
[53] D.K. Shen, S. Gu, K.H. Luo, A.V. Bridgwater, Analysis of wood structural changes under thermal radiation, Energy Fuel. 23 (2009) 1081–1088, https://doi.org/10.1021/ef800873k.
[54] D. Drysdale, The post-flashover compartment fire, Introd. Fire Dyn. (2011) 387–439, https://doi.org/10.1002/9781119975465.ch10.
[55] I. Oleszkiewicz, Heat transfer from a window fire plume to a building facade, Pap. (National Res. Counc. Canada. Inst. Res. Constr. No. IRC-P-1662, https://doi.org/10.4224/40001813, 1989.
[56] P.H. Thomas, M. Law, The Projection of Flames from Burning Buildings - FRN No. 921, 1972.